PNAS

Supplementary Information (SI) Appendix for

A next-generation intranasal trivalent MMS vaccine induces durable and broad protection against SARS-CoV-2 variants of concern

Jiayu Xu[a,1], Yuexiu Zhang[a,1], Panke Qu[a,2], Mohamed M. Shamseldin[b,c,2], Sung J. Yoo[a,2], Jack Misny[d,2], Ilada Thongpan[d], Mahesh KC[d], Jesse M. Hall[b], John P. Evans[a], Mostafa Eltobgy[b], Mijia Lu[a], Chengjin Ye[e], Michelle Chamblee[a], Xueya Liang[a], Luis Martinez-Sobrido[e], Amal O Amer [b,f], Jacob S Yount[b,f], Prosper N Boyaka[a,f], Mark E. Peeples[d, f, g], Shan-Lu Liu[a,b,f,h], Purnima Dubey[b,f], Jianrong Li[a,f, 3]

[a]Department of Veterinary Biosciences, The Ohio State University, Columbus, OH 43210
[b]Department of Microbial Infection and Immunity, College of Medicine, The Ohio State University, Columbus, OH 43210
[c]Department of Microbiology and Immunology, Faculty of Pharmacy, Helwan University, Ain Helwan, Helwan, 11795, Egypt
[d]Center for Vaccines and Immunity, Abigail Wexner Research Institute at Nationwide Children's Hospital, Columbus, OH 43205
[e] Department of Disease Intervention and Prevention, Texas Biomedical Research Institute, San Antonio, TX, USA 78227
[f]Department of Pediatrics, College of Medicine, The Ohio State University, Columbus, OH 43210
[g]Infectious Disease Institute, The Ohio State University, Columbus, OH 43210
[h]Center for Retrovirus Research, The Ohio State University, Columbus, OH 43210

[1] J.X. and Y. Z. contributed equally to this work. [2]P.Q., M.M.S., S.J.Y., and J.M. contributed equally to this work.

[3]Corresponding author
Department of Veterinary Biosciences
College of Veterinary Medicine
The Ohio State University
1925 Coffey Road
Columbus, OH 43210
Phone: (614) 688-2064; Email : li.926@osu.edu

This PDF file includes:

Supplementary Materials and Methods
Figures S1 to S11
Additional discussion
SI References

Supplementary Materials and Methods

Cell culture. Vero CCL81 cells (African green monkey, ATCC no. CCL81), HEp-2 cells (ATCC no. CCL-23), Vero-TMPRSS2 cells (BEI, NR-54970), and HEK293T-ACE2 cells (BEI, NR-52511) were grown in Dulbecco's modified Eagle's medium (DMEM; Life Technologies) supplemented with 10% fetal bovine serum (FBS). FreeStyle293F cells (Thermo Fisher) were grown in protein-free medium in suspension culture.

Animals. Specific-pathogen-free (SPF) interferon-alpha receptor 1 knockout ($IFNAR1^{-/-}$) mice were purchased from Jackson Laboratories (Bar Harbor, ME). 4-6-week-old SPF golden Syrian hamsters were purchased from Envigo (Indianapolis, IN).

SARS-CoV-2 stocks. The SARS-CoV-2 USA-WA1/2020 natural isolate (SARS-CoV-2 WA1, NR-52281) was obtained from BEI Resources. The SARS-CoV-2 WA1 was originally isolated from an oropharyngeal swab from a patient with respiratory illness in January 2020 in Washington, USA. SARS-CoV-2 Delta (B.1.617.2) variant was originally isolated in the US and obtained from BEI Resources (NR-55671). SARS-CoV-2 Omicron BA.1 were kindly provided by Dr. Luis Martinez-Sobrido. All viruses were amplified and titrated on Vero-TMPRSS2 cells to prevent the selection of SARS-CoV-2 viruses lacking their furin cleavage site between spike 1 (S1) and S2. All experiments with SARS-CoV-2 virus were performed in a BSL3 facility.

Design of prefusion spike with 6 prolines (preS-6P). The design of preS-6P of Delta and

Omicron BA.1 variants is the same as the SARS-CoV-2 WA1 preS-6P (1). The six amino acids (K986, V987, F817, A892, A899, and A942) in the S2 portion of the S head region replaced with prolines (6P), the furin cleavage site deleted to prevent S1–S2 cleavage, and its C-terminal transmembrane/cytoplasmic tail domain is replaced with a T4 fibritin self-trimerizing domain.

Rapid assembly of the full-length genomic cDNA of mumps virus (MuV) and measles virus (MeV) using a yeast-based recombination system. The full-length genomic cDNA of MuV Jeryl Lynn (JL1) vaccine strain was synthesized by five overlapping DNA fragments and assembled into the pYES2 vector (2-4). The pYES2 vector contains a yeast replication origin, a T7 RNA polymerase promoter positioned before the full-length MuV genome cDNA, which was followed by a hepatitis delta virus ribozyme (HDVRz) and a T7 terminator sequences. The full-length cDNA clone of MuV-JL1 was assembled using 6 overlapping fragments and an additional 7th fragment of preS-6P (Delta variant) by using a yeast recombination system. Briefly, 100 ng of pYES2 vector was mixed with 100 ng of each MuV and preS-6P DNA fragment in a PEG/LiAc solution, and the ligation products were transformed into MaV 203 competent yeast cells by heat-shock and plated on SD/Ura$^-$ agar plates. The plates were incubated at 30℃ for 3 days. Individual yeast colonies were picked and grown in SD/Ura$^-$ broth at 30℃ overnight. DNA was extracted from yeasts using Qiagen mini-prep kit. The connecting regions between fragments of the plasmids were amplified by PCR and sequenced, and the positive plasmids were transformed into TOP10 *E. Coli*. competent cells. Subsequently, plasmid DNA was extracted from bacterial culture and verified by Hind III restriction enzyme digestion, PCR analysis, and then sequenced to confirm that no additional mutations had been introduced during the assembly. The final plasmid was designated as pMuV-JL1-Delta-preS-6P.

Using the same method, the full-length cDNA clone of Edmonston strain of MeV vaccine was constructed using six overlapping fragments and an additional 7th fragment of preS-6P (Omicron BA.1) by using yeast recombination system (2-4), the plasmid was designated as pMeV-BA.1-preS-6P. Primers used for amplification of MeV and MuV cDNA fragments were listed in our previous publications (2, 4).

Recovery of rMuV-JL1-Delta-preS-6P and rMeV-BA.1-preS-6P. Recovery of rMeV-BA.1-preS-6P and rMuV-JL1-Delta-preS-6P from the infectious clone was carried out as described previously (2-4). For the rMuV-JL1-Delta-preS-6P recovery, a plasmid encoding the full-length genome of MuV JL1 strain with the preS-6P (Delta) gene inserted and support plasmids encoding the MuV-JL1 genome-associated ribonucleocapsid complex (pN, pP, and pL) were co-transfected into HEp-2 cells infected with a recombinant modified vaccinia Ankara virus (MVA-T7) expressing T7 RNA polymerase (kindly provided by Dr. Bernard Moss) at an multiplicity of infection (MOI) of 10 (5). For the rMeV-BA.1-preS-6P recovery, a plasmid encoding the full-length genome of MeV strain with the preS-6P (Omicron BA.1) gene inserted and support plasmids (pN, pP, and pL) were co-transfected into HEp-2 infected with MVA-T7 at an MOI of 10. Four-day later, the transfected cells were scraped off the plates and co-cultured with fresh Vero CCL81 cells. After 4-5 days, cells were harvested and used for the next passage to further amplification of the recovered recombinant viruses. Subsequently, the recovered viruses were plaque purified. Individual plaques were isolated, and seed stocks were amplified in Vero CCL81 cells. Seed stocks were passed 2-3 times in Vero CCL81 cells. Large stock of virus was grown in 10 T150 flask, purified, and viral titers were determined by plaque assay in Vero CCL81 cells.

RT-PCR and sequencing. Viral RNA was extracted from rMeV-BA.1-preS-6P and rMuV-JL1-Delta-preS-6P stocks with a RNeasy minikit (Qiagen, Valencia, CA) according to the manufacturer's instructions. SARS-CoV-2 preS-6P gene, MuV, or MeV DNA fragments were amplified by a One Step RT-PCR kit (Qiagen). The amplified DNA products were purified in 1% agarose gel electrophoresis and sequenced to confirm that preS-6P was inserted into the MuV or MeV genome and that no additional mutations were introduced during virus recovery and passages.

MeV or MuV-JL1 growth curves. Vero CCL81 cells were seeded in 12-well-plates. After overnight incubation, confluent Vero CCL81 cells were infected with individual virus at a MOI of 0.1. After 1 h of adsorption in a rocker at 37°C incubator, the inoculum was removed, the cells were washed two times with fresh DMEM, and DMEM with 2% FBS was added. After that, the infected cells were incubated at 37°C. At the indicated time points, cell culture supernatant was harvested, and virus titers were determined by plaque assay in Vero CCL81 cells.

Plaque assays. For MuV and MeV plaque assay, Vero CCL81 cells were seeded in 12-well plates. After overnight incubation at 37°C, confluent monolayer cells were infected with 10-fold serial dilutions of virus stock of MuV or MeV. After adsorption for 1 h at 37°C, cells were overlaid with 1 ml of DMEM containing 0.25% (w/v) low-melting agarose, 0.12% (v/v) $NaHCO_3$, 2% (v/v) FBS, 25mM HEPES, 2mM L-Glutamine, 100µg/ml of streptomycin, and 100U/ml penicillin. The plates were incubated at 37°C for 4 days, and cells were fixed with 4% paraformaldehyde for 1 h.

After fixation, the overlay was discarded, and viral plaques were visualized by staining with 0.05% (v/v) crystal violet. The protocol for SARS-CoV-2 plaque assay was similar to that of MuV and MeV except that the assay was performed on Vero TMPRSS2 cells and the incubation time was 2 days.

Detection of SARS-CoV-2 S protein by Western blot. Vero CCL81 cells were infected with parental rMeV or rMeV-BA.1-preS-6P, rMuV-JL1 or rMuV-JL1-Delta-preS-6P, rMuV-JL2 or rMuV-JL2-WA1-preS-6P at an MOI of 0.1. At the indicated times post-infection, supernatant was collected and cells were lysed in RIPA buffer (Abcam, ab156034) and boiled for 5 min at 100 °C. The proteins were loaded under non-reduced conditions on 12% SDS-PAGE and transferred to a Hybond enhanced chemiluminescence nitrocellulose membrane (Amersham) in a Mini Trans-Blot electrophoretic transfer cell (Bio-Rad). The membrane was incubated with rabbit anti-SARS-CoV-2 S polyclonal antibody (SinoBiological, 40150-T62-COV2) at a dilution of 1:2,000, and β-actin at a dilution of 1:5,000, followed by incubation with horseradish peroxidase (HRP)-labeled goat anti-rabbit and anti-mouse secondary antibody at a dilution of 1:5,000 in 5 % skim milk. The membrane was developed using an Odyssey CLx (LI-COR, Lincoln, NE).

Virus neutralization assay. Virus neutralization assays were performed as previously described (6). Mice or hamster sera samples were heat inactivated at 56°C for 30 min. Briefly, sera were 4-fold serially diluted in DMEM in a 96-well plate and equal amounts of SARS-CoV-2 variant pseudotyped virus was added to the diluted serum to get final dilutions of 1:40, 1:160, 1:640, 1:2560, 1:10240, and no serum control. The pseudoviruses including D614G, Delta (B.1.617.2) (7), Omicron BA.1, and BA.4/5 (8) were incubated with serum 1 h at 37°C, followed by infection

of 2×10^4 pre-seeded HEK293T-ACE2 cells on a 96-well polystyrene tissue culture plate (6). Gaussia luciferase activity in cell culture media was assayed 48 h and 72 h after infection. Luminescence was immediately measured by combining 20 μL cell culture media with 20 μL of *Gaussia* luciferase substrate (0.1 M Tris pH 7.4, 0.3 M sodium ascorbate, 10 μM coelenterazine) on a BioTek Cytation5 plate reader. To ensure valid comparisons between SARS-CoV-2 variants and ancestral strains, equivalent amounts of infectious pseudoviruses were used based on the pre-determined virus titers and samples of different variants were loaded side by side in each plate. Neutralizing titer 50% (NT_{50}) for each sample was determined by non-linear regression with least squares fit in GraphPad Prism 9 (San Diego, CA).

Detection of SARS-CoV-2-specific serum IgG and lgA antibody by ELISA. Serum IgG and IgA antibodies were detected by ELISA as described in our previous publication (3). Briefly, ninety-six-well plates were coated with 8 μg/ml prefusion S protein (preS-6P) of SARS-CoV-2 WA1, BA.1 or Delta (in 50 mM Na_2CO_3 buffer, pH 9.6) at 4°C overnight. The plates were washed one time with phosphate-buffered saline containing 0.05% Tween-20 (PBST) and blocked with 1% (w/v) Bovine Serum Albumin (BSA) in PBS at 4°C overnight. Each serum sample was 4-fold serially diluted in blocking buffer and added to the preS-6P protein-coated wells (100 μl/well). The plates were incubated at room temperature for 2h, washed three times with PBST, and incubated with 100 μl/well of 1:15,000 blocking buffer-diluted horseradish peroxidase (HRP)-conjugated secondary antibody (goat anti-mouse IgG (H+L) (Thermo Scientific, catalog no. 31430) or goat anti-hamster IgG (H+L) (Invitrogen, catalog no. PA1-28823) at room temperature for 1 h. The SARS-CoV-2 S-specific IgA antibody was detected by adding HRP-conjugated anti-mouse IgA (Southern Biotech Associates Inc., Birmingham, AL) or HRP-conjugated anti-Hamster

IgA (Brookwoodbiomedical, Jemison, AL). The SARS-CoV-2 S-specific IgG antibody was detected by adding 100 µl/well of SureBlue™ TMB 1-Component Microwell Peroxidase Substrate (Fisher Scientific, 50-674-93), and stopped by 100µl of H_2SO_4 (2 mol/L). Optical densities at 450 nm (OD_{450}) were measured by a BioTek microplate reader. Endpoint titers were determined as the reciprocal of the highest dilution that had an OD_{450} value 2.1-fold greater than the background level (normal control serum).

Animal experiments: All animals were housed within ULAR facilities of The Ohio State University under approved Institutional Laboratory Animal Care and Use Committee (IACUC) guidelines (protocol no. 2009A1060-R3 and 2020A00000053). Each inoculation group was separately housed in rodent cages under animal biosafety level 2 (ABSL-2 for MeV and MuV) or ABSL3 (for SARS-CoV-2) conditions.

Animal experiment 1: To compare the efficacy of the monovalent (rMeV-BA.1-preS-6P) and the trivalent vaccine (rMeV-BA.1-preS-6P, rMuV-JL1-Delta-preS-6P, and rMuV-JL2-WA1-preS-6P) in IFNAR1$^{-/-}$ mice. Twenty-five 4-week-old IFNAR1$^{-/-}$ mice (Jackson Laboratory, Bar Harbor, ME) were randomly divided into 5 groups (n=5). Mice in groups 1-3 were immunized with 1.5×10^6 PFU (high dose) of monovalent, trivalent, or parental rMeV, rMuV-JL1, and rMuV-JL2 respectively. The administration route was 7.5×10^5 PFU in 30µL of DMEM for intranasal (*i.n.*) combined with 7.5×10^5 PFU in 500µL of DMEM for subcutaneous (*s.c.*). Three weeks later, all mice were boosted with the same virus by the same dose and route of immunization. At weeks 2, 5, and 7, blood samples were collected from each mouse from the facial vein. Serum was isolated and used to detect WA1, Delta, or BA.1 S-specific IgG and lgA antibody by ELISA, the serum at

week 7 was used to detect neutralization antibody against WA1-D614G, Delta, Omicron BA.1, and BA4/5 pseudotyped virus. At week 4 post booster immunization, mice in groups 1-3 were sacrificed, lung and spleens were collected for T cell assay.

Mice in groups 4-5 were immunized with 5×10^5 PFU (low dose) of monovalent rMeV-BA.1-preS-6P and trivalent (half for intranasal and half for subcutaneous). Three weeks later, all mice were boosted with the same virus by the same dose and route of immunization. At weeks 2, 5, 7, 11, 13, and 16 weeks, blood samples were collected from each mouse from the facial vein. Serum was isolated and used to detect WA1, Delta, or BA.1 S-specific IgG antibody by ELISA.

Animal experiment 2: To determine the efficacy of the monovalent (rMeV-BA.1-preS-6P) and the trivalent vaccine in golden Syrian hamsters. Fifty 4-week-old female SPF golden Syrian hamsters were randomly divided into 4 groups. Hamster in Group 1 (*n*=15) were inoculated with 1.5×10^6 PFU rMeV-BA.1-preS-6P. Hamster in Group 2 (*n*=15) were inoculated with 1.5×10^6 PFU trivalent vaccine. Hamster in Group 3 (*n*=15) and Group 4 (*n*=5) were immunized with 1.5×10^6 PFU parental MMM vector, or the same volume of DMEM, respectively. The administration route was 7.5×10^5 PFU in 30μL of DMEM for intranasal (*i.n.*) combined with 7.5×10^5 PFU in 500μL of DMEM for subcutaneous (*s.c.*). Three weeks later, all hamsters were boosted with the same virus by the same dose and route of immunization. At weeks 2, 5, and 7, blood samples were collected from each hamster via retro-orbital plexus, serum was isolated, and S-specific antibody against WA1, Delta, and BA.1 was detected by ELISA. The serum at week 7 was isolated to detect neutralization antibody against WA1-D614G, Delta, Omicron BA.1, and BA4/5 pseudotyped virus.

224

225 At week 4 post-booster immunization, hamsters in groups 1-3 were transferred into the BSL3
226 facility and each group were divided into 3 subgroups (*n*=5) and challenged with 2×10^4 PFU of
227 SARS-CoV-2 USA-WA1/2020 strain WA1, 2×10^4 PFU Delta, and 7×10^5 PFU Omicron BA.1. We
228 slightly adjusted the challenge protocol for Omicron BA.1 because previous studies suggested that
229 hamsters are less susceptible to Omicron BA.1 infection probably due to the alteration of its
230 receptor binding affinity to hamster ACE2 (9). To overcome this problem, hamsters were
231 intranasally infected with 10^8 PFU of Ad5-hACE2 5 days prior to being challenged with BA.1
232 virus. Hamsters in group 4 were inoculated with DMEM and served as unimmunized unchallenged
233 controls and maintained in the BSL2 facility. After SARS-CoV-2 challenge, clinical signs and body
234 weight of each hamster were monitored daily. At day 4 (WA1 and Delta) or day 3 (Omicron BA.1)
235 post-challenge, all hamsters in each group were euthanized, and left lung and nasal turbinate were
236 collected for detection of infectious SARS-CoV-2 by plaque assay. In addition, the right lung was
237 preserved in 4% (v/v) phosphate-buffered formaldehyde for histology.

238

239 **Animal experiment 3:** To determine whether intranasal immunization alone can provide
240 protection against SARS-CoV-2 challenge. Thirty five 4-week-old female SPF golden Syrian
241 hamsters were randomly divided into 7 groups (*n*=5). Hamsters in groups 1-3 were inoculated with
242 1.5×10^6 PFU trivalent vaccine by intranasal route. Hamsters in groups 4-6 were immunized with
243 1.5×10^6 PFU parental MMM vector by intranasal route. Hamsters in group 7 were immunized
244 with the same volume of DMEM by intranasal route. Two weeks later, all hamsters were boosted
245 with the same virus by the same dose and route of immunization. At weeks 2, 4, and 6, blood
246 samples were collected from each hamster via retro-orbital plexus, serum was isolated, and S-

specific IgG and IgA antibodies against WA1, Delta, and BA.1 were detected by ELISA. At week 5 post-booster immunization, hamsters in groups 1-6 were transferred into the BSL3 facility. Hamsters in groups 1 and 4, groups 2 and 5, and groups 3 and 6 were challenged with 2×10^4 PFU SARS-CoV-2 USA-WA1/2020 strain WA1, 2×10^4 PFU Delta, and 7×10^5 PFU Omicron BA.1, respectively. For SARS-CoV-2 Omicron BA.1 infection, hamsters were intranasally infected with 10^8 PFU of Ad5-hACE2 5 days prior to being challenged with BA.1 virus. Hamsters in group 7 were inoculated with DMEM and served as unimmunized unchallenged controls and maintained in the BSL2 facility. After SARS-CoV-2 challenge, clinical signs and body weight of each hamster were monitored daily. At day 4 (WA1 and Delta) or day 3 (Omicron BA.1) post-challenge, all hamsters in each group were euthanized, and lung and nasal turbinate were collected for detection of infectious SARS-CoV-2 by plaque assay.

Animal experiment 4: To compare the efficacy of the immunization route. Twenty 4-6-week-old SPF female IFNAR1$^{-/-}$ mice (Jackson Laboratory, Bar Harbor, ME) were randomly divided into 2 groups (n=10). Mice in group 1 and group 2 were immunized intranasally or subcutaneously with 1.2×10^6 PFU of trivalent vaccine, respectively. Two week later, all mice were boosted with the same virus at same dose and route. At weeks 2, 4, and 6, blood samples were collected from each mouse by facial vein bleeding, serum isolated, and WA1, Delta, or BA.1 S-specific IgG and IgA antibodies were detected by ELISA. At weeks 6, mice were euthanatized. Lung bronchoalveolar lavage (BAL) were collected, WA1, Delta, or BA.1 S- specific IgG or IgA in BAL were measured by ELISA.

Animal experiment 5: To determine whether rMeV and rMuV vectors interfere with S-specific

antibody induced by rMuV-JL1-Delta-preS-6P. Twenty 4-week-old IFNAR1$^{-/-}$ mice (Jackson Laboratory, Bar Harbor, ME) were randomly divided into 4 groups (n=5). Mice in group 1 were immunized with 1.5×10^6 PFU of trivalent vaccine (a mixture of 5×10^5 PFU of rMeV-BA.1-preS-6P, 5×10^5 PFU of rMuV-JL1-Delta-preS-6P, and 5×10^5 PFU of rMuV-JL2-WA1-preS-6P) by intranasal route. Mice in group 2 were immunized with 1.5×10^6 PFU of rMuV-JL1-Delta-preS-6P by intranasal route. Mice in group 3 were immunized with 5×10^5 PFU of rMuV-JL1-Delta-preS-6P by intranasal route. Mice in group 4 were immunized with 1.5×10^6 PFU of a mixture of rMuV-JL1-Delta-preS-6P, rMuV-JL2, and rMeV (5×10^5 PFU of rMuV-JL1-Delta-preS-6P, 5×10^5 PFU of rMuV-JL2, and 5×10^5 PFU of rMeV) by intranasal route. Two week later, all mice were boosted with the same virus by the same dose and route of immunization. At weeks 2, 4, and 6, blood samples were collected from each mouse from the facial vein. Serum was isolated and used to detect WA1, Delta, or BA.1 S-specific IgG antibody by ELISA.

Recombinant antigen production. The plasmid pCAGGS encoding the SARS-CoV-2 WA1, Delta, and BA.1 stabilized soluble preS-6P protein (amino acids 1-1273) was transfected into FreeStyle293F cells to produce the preS-6P protein. After transfection, cell culture supernatants were collected and the secreted preS-6P protein was purified via affinity chromatography as described (1). The purified proteins were analyzed by SDS-PAGE and visualized by Coomassie blue staining. Protein concentration was measured using Bradford reagent (Sigma Chemical Co., St. Louis, MO).

Analysis of resident and circulating T cells in the lungs. IFNAR1$^{-/-}$ mice immunized with 1.5×10^6 PFU (high dose) of monovalent, trivalent, or parental rMeV, rMuV-JL1, and rMuV-JL2

were terminated at week 7. To discriminate the circulating T cells from the resident T cells in the lungs, anti-CD45-PE (Clone 30-F11, BD Biosciences) (3 μg in 100 μL sterile PBS) was retro-orbitally injected into mice 10 min prior to euthanasia. The circulating lymphocytes were labeled by anti-CD45-PE antibody whereas resident lymphocytes are protected from labeling. Peripheral blood was collected at time of sacrifice and analyzed by flow cytometry to confirm that >90% of circulating lymphocytes were CD45-PE^{+} and ensure that the tissue resident CD45- cells in the tissues are tissue resident.

At the termination, lungs were isolated and homogenized into a single cell suspension using the gentleMACS tissue dissociator and mouse lung dissociation kit (Miltenyi Biotec Ref. 130-095-927). The cell suspensions were filtered using 40 μm filter and red blood cells were removed using ACK lysis buffer. Cell suspensions were processed in the dark to minimize photobleaching of the CD45-PE signal. After that, cells were resuspended in T cell media (RPMI 1640 supplemented with 0.1% gentamicin antibiotic, 10% HI-FBS, Glutamax, and 5×10^{-5} M β-ME) and incubated for 4-5 h at 37°C with protein transport inhibitor cocktail (eBioscience). Subsequently, cells were stimulated with PMA (50 ng/ml) /Ionomycin (500 ng/ml) or with two S peptide pools covering the C- and N-terminus of SARS-CoV-2 S protein (PepTivator SARS-CoV-2 Prot_S1 and PepTivator SARS-CoV-2 Prot_S+) (Miltenyi Biotec Ref. 130-126-701& 130-126-700). The final concentration of each peptide is 1 μg/ml. For negative controls, cells incubated with DMSO alone. The peptide stimulation time should not affect CD45-PE staining. This method has been validated by Anderson KG et al (2014) (10).

After stimulation, cells were washed with cold PBS followed by staining with LIVE/DEAD

316 Zombie NIR Fixable Viability dye (Biolegend Cat. 423105) for 30 min at 4°C. Cells were then
317 washed twice with PBS supplemented with 1% HI-FBS (1% FBS) (FACS buffer) and resuspended
318 in Fc Block (clone 93) (eBioscience Ref. 14-0161-86) at 4°C for 5 min before surface staining
319 with a cocktail of the following antibodies for 20 min at 4ºC: CD4 BV750 (Clone H129.19) (BD
320 Cat. 747275), CD44 PerCP Cy5.5 (Clone IM7) (BD Cat. 560570), CD62L BV605 (Clone MEL-
321 14) (BD Cat. 563252) and CD69 BV711 (Clone HI.2F3) (BD Cat. 740664). After two washes in
322 FACS buffer cells were resuspended in IC fixation buffer (eBioscience Cat. 00-8222-49) and
323 incubated for 20 min at room temperature. Then, cells were permeabilized (eBioscience Cat. 00-
324 8333-56), followed by intracellular staining for 30 min at 4°C using a cocktail of the following
325 antibodies: IL-17 PE CY7 (clone eBio17B7) (eBioscience Cat. 25-7177-82), IFNγ FITC (clone
326 XMG1.2) (eBioscience Cat. 11-7311-82), and IL-5 APC (clone TRFK5) (BD Cat. 554396). To
327 detect the CD8+ T cell population, the same panel was used with the replacement of CD4 BV750
328 antibody with CD8 APC (clone 53-6.7) (Biolegend Cat. 100712) and probing for IFNγ only. For
329 negative controls, fluorescence minus one or isotype control antibodies were used. Finally, cells
330 were washed with permeabilization buffer and resuspended in FACS buffer. Samples were
331 collected on a Cytek Aurora flow cytometer (Cytekbio). Flow cytometer data analysis was
332 performed using FlowJo software (version 10.8.0). The number of cells within each population
333 was calculated by multiplying the frequency of live singlets in the population of interest by the
334 total number of cells in each sample. Gating strategy for PMA/Ionomycin and S peptide
335 stimulation was shown in **Fig.S2** and **Fig.S3**, respectively.
336
337 **Flow cytometry analysis of antigen-specific cytokine producing T cells in spleen.** IFNAR1$^{-/-}$
338 mice immunized with 1.5×10^6 PFU (high dose) of monovalent, trivalent, or parental rMeV, rMuV-

JL1, and rMuV-JL2 were terminated at week 7 for analyzing T cells in the spleen. For this purpose, 10^6 spleen cells were stimulated with 5 μg/ml of preS-6P protein *in vitro* for 5 days in 96-well round bottom plates. Cells were then cultured for 4 h in the presence of PMA/Ionomycin (BioLegend) and GolgiStop (BD Biosciences). Following incubation, cells were surface stained for CD3, CD4, and CD8 for 30 min at 4°C, fixed and permeabilized using the cytofix/cytoperm kit (BD Biosciences), and intracellularly stained for IFN-γ, TNF-α, IL-4, IL-10, IL-17, and IL-21 for 30 min at room temperature. The following mouse reactive antibodies (clone, catalog number, dilution) from BioLegend, BD Biosciences, and ThermoFisher Scientific were used for analysis of T cells: CD3-PE/Cyanine7 (145-2C11, 100319, 1:400), TNFα-Brilliant Violet 785 (MP6-XT22, 506341, 1:400), IFNγ-PE/Dazzle 594 (XMG1.2, 505845, 1:400), IL-4-Brilliant Violet 711 (11B11, 504133, 1:100), IL-21 Alexa Fluor 647 (mhalx21, 51-7213-80, 1:100), IL-17 Alexa Fluor 488 (TC11-18H10, 560221, 1:100), CD8-BUV737 (53-6.7, 612759, 1:400), CD4-BUV 496 (GK1.5, 612952, 1:400), and IL-10-Brilliant Violet 510 (JES5-16E3, 563277, 1:100). The cells were analyzed with an Attune flow cytometer and data analyzed using FlowJo v10. Gating strategy was shown in **Fig.S8**.

Determination of SARS-CoV-2 viral titer in tissues. At day 3 or 4 after SARS-CoV-2 challenge, animals were terminated. The left lung lobe and nasal turbinate were collected and stored at -80°C. Tissues were weighed and homogenized by hand with a mortar and pestle (Golden, CO) in 1mL of sterile PBS. The presence of infectious SARS-CoV-2 was determined by plaque assay in Vero-TMPRSS2 cells.

Histological analysis of lung tissues. At the termination of animals, the right lung lobe was

362 preserved in phosphate-buffered 4% (v/v) formaldehyde for 14 days and then transferred out of
363 the BSL-3 facility. Fixed lung tissues were embedded in paraffin, sectioned at 5 μm in duplicate,
364 deparaffinized, and rehydrated. Each section was stained with hematoxylin-eosin (H.E.) and sent
365 to a pathologist for blind review of histological changes. Each lung section was scored based on
366 the severity of histologic changes. Score 4 = extremely severe; score 3 = severe; score 2 =
367 moderate; score 1 = mild; score 0 = no pathological changes.
368
369 **Statistical analysis.** Statistical analysis was performed by Student's *t*-test, one-way or two-way
370 ANOVA multiple comparisons using GraphPad Prism software (San Diego, CA). A *P* value of
371 <0.05 was considered statistically significant.
372
373
374
375
376
377
378
379
380
381
382
383
384

Supplementary figures 1-11

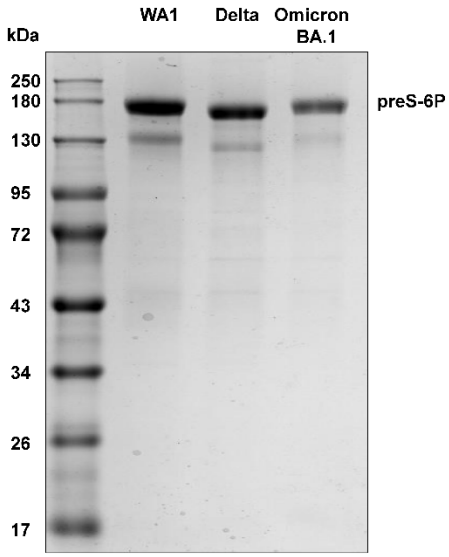

Fig.S1. SDS-PAGE analyses for purified SARS-CoV-2 preS-6P protein. The preS-6P of SARS-CoV-2 WA1, Delta variant, and Omicron BA.1 were purified and analyzed by SDS-PAGE followed by Coomassie blue staining.

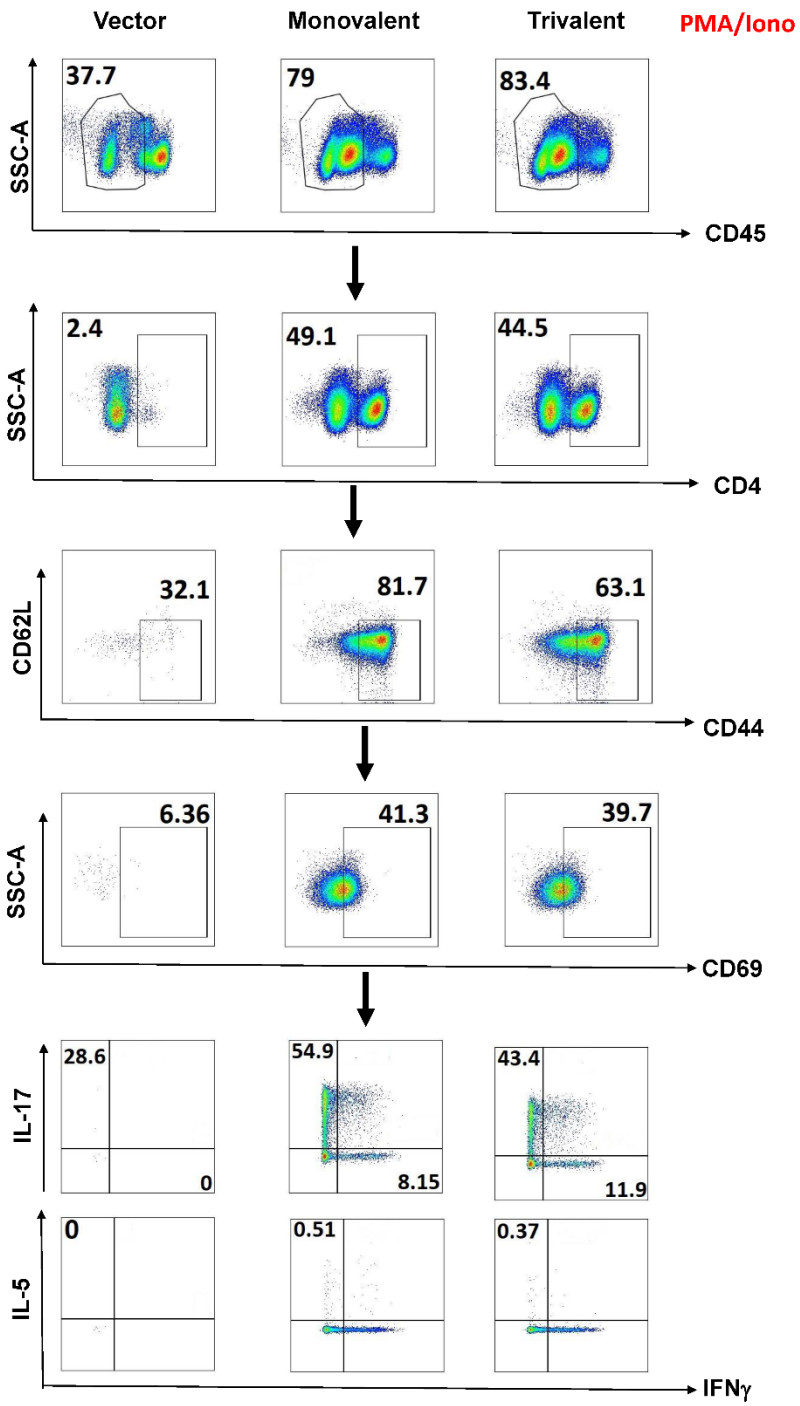

393

394

395 **Fig.S2. Gating strategy for characterization of lung-resident CD4$^+$ T cells producing**

396 **cytokines after stimulation with PMA/Ionomycin in intracellular cytokine staining (ICS)**

397 **assay.**

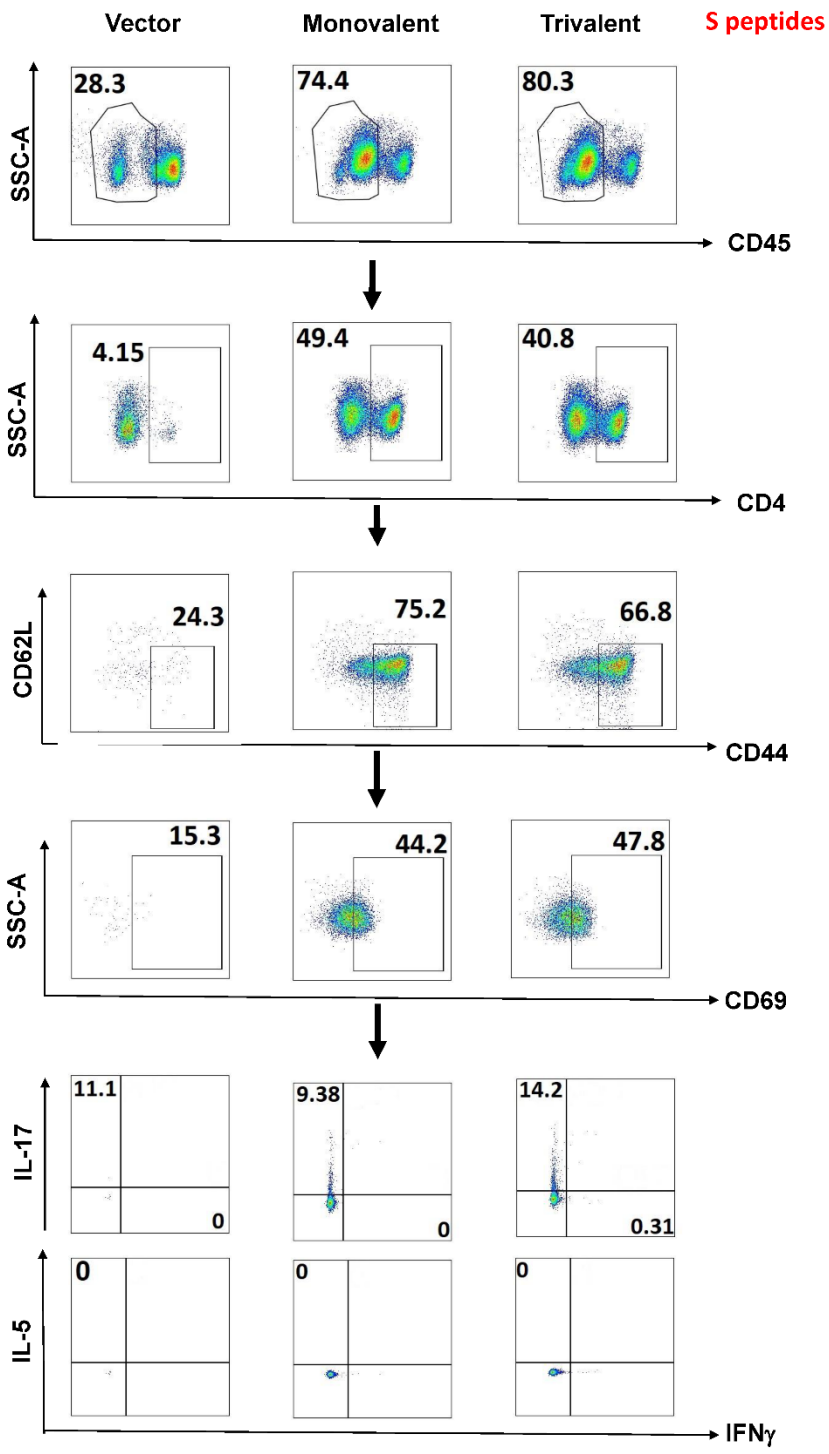

398

399 **Fig.S3. Gating strategy for characterization of S peptide-specific CD4$^+$ T cells producing**

400 **cytokines after stimulation with SARS-CoV-2 S peptide in intracellular cytokine staining**

401 **(ICS) assay.**

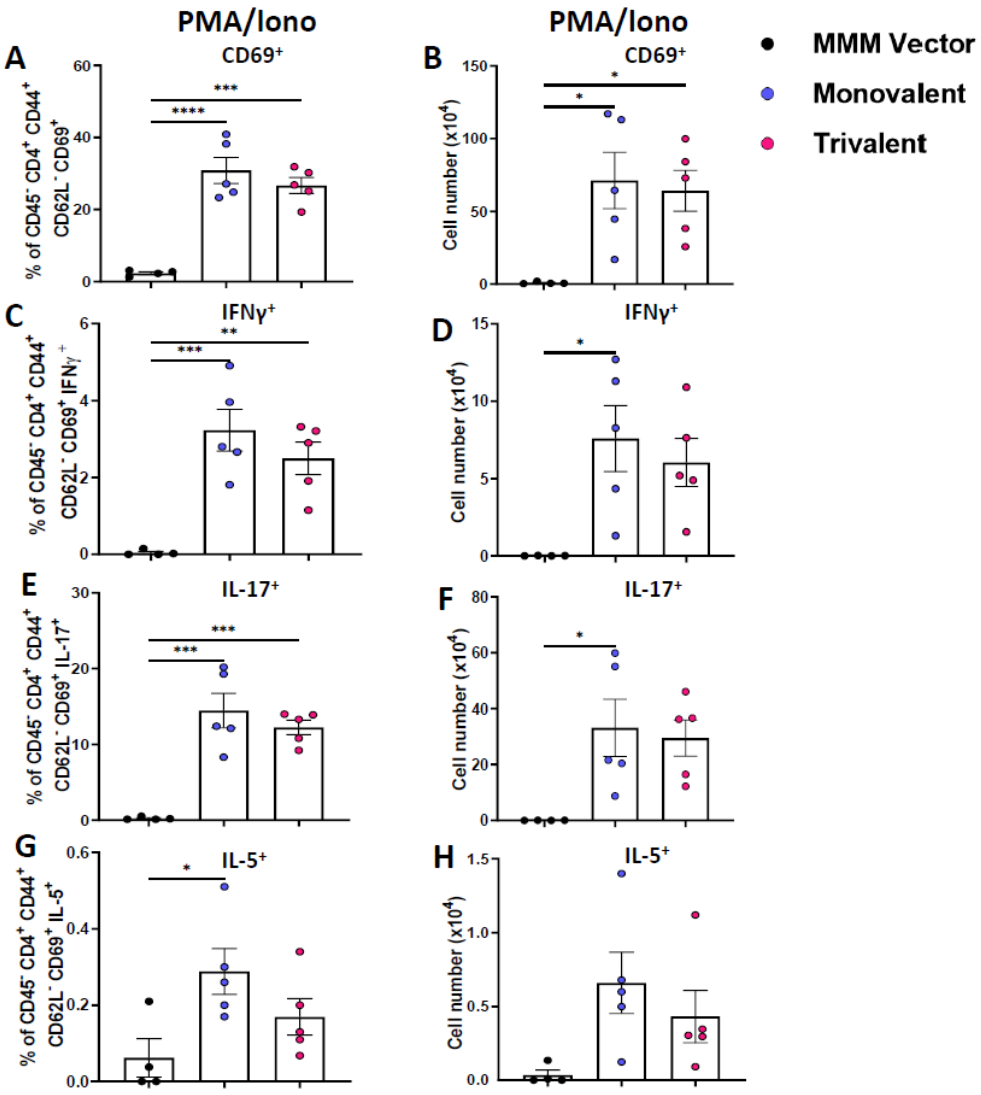

Fig.S4. Monovalent and trivalent vaccines induce tissue-resident CD4$^+$ T cell immune responses in the lungs after stimulation with PMA/Ionomycin. Lung CD45$^-$ T cell suspensions from **Fig.5** were stimulated with PMA/Ionomycin in the presence of protein transport inhibitors. The percent and number of PMA/Ionomycin-stimulated CD45$^-$ CD4$^+$CD44$^+$CD62L$^-$CD69$^+$ T cells (A and B), IFNγ$^+$ (C and D), IL-17$^+$ (E and F), and IL-5$^+$ (G and H) producing CD4$^+$ T cells are shown. One-way ANOVA with Tukey's multiple comparisons was used to detect differences among groups (*$P < 0.05$; **$P < 0.01$; ***$P < 0.001$; ****$P < 0.0001$).

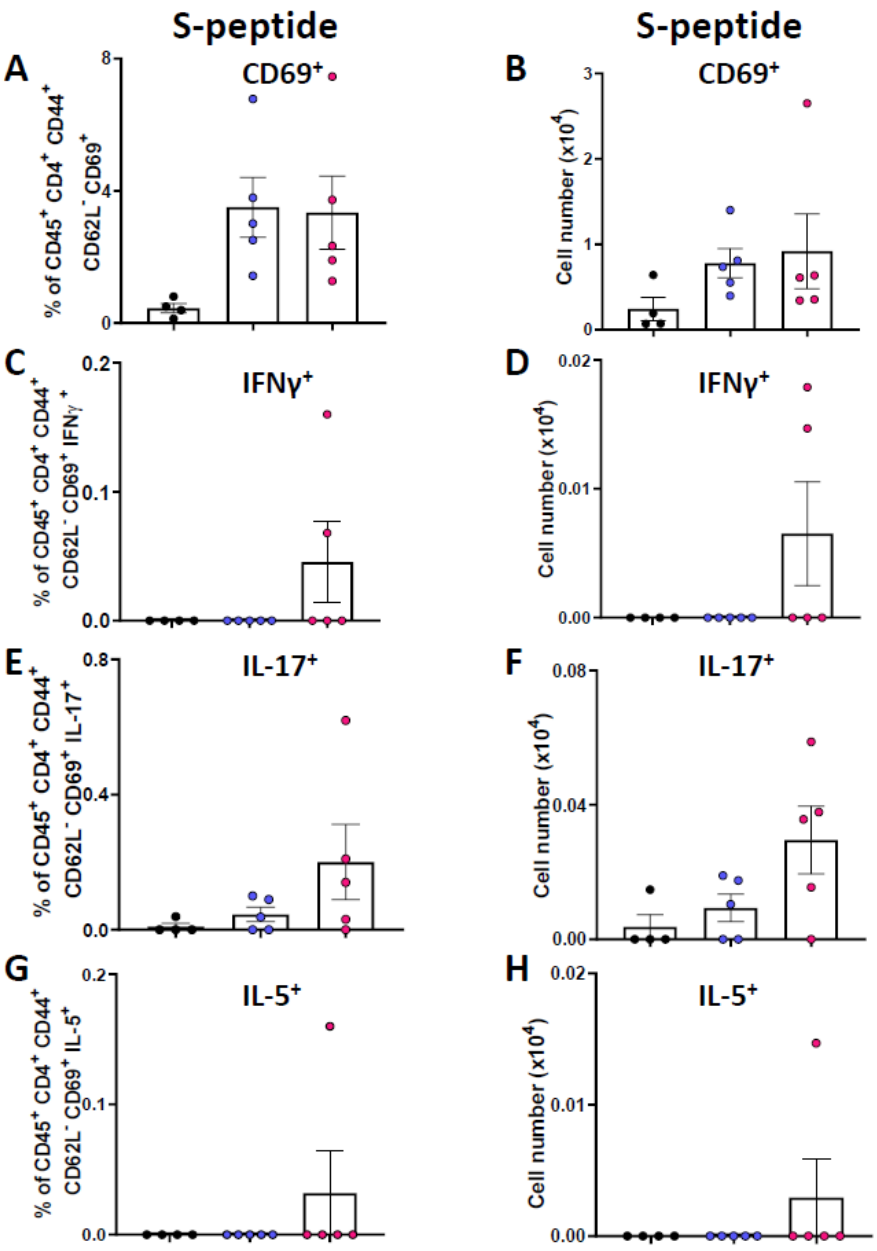

411

412

413

414

415

416

417

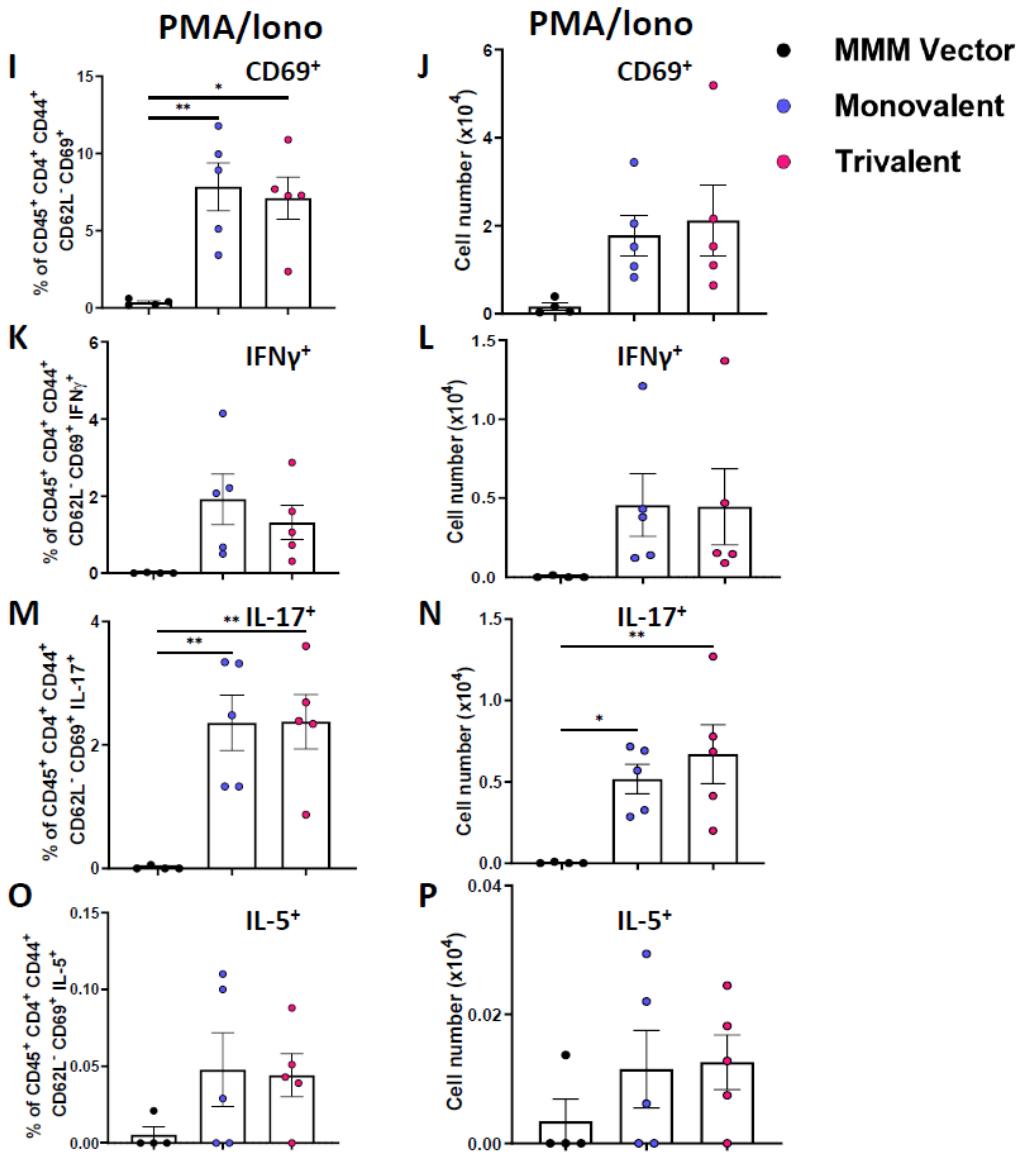

Fig.S5. Monovalent and trivalent vaccines induce circulating CD4$^+$ T cell immune responses in the lungs. Lung CD45$^+$ T cell suspensions were stimulated with an S-specific peptide pool (A-H) or PMA/Ionomycin (I-P) in the presence of protein transport inhibitors. Cells were surface stained with antibodies specific for CD4 or CD8, CD62L, CD44, CD69, then fixed, permeabilized, and stained with anti- IFNγ, anti-IL-17, and anti-IL-5 for CD4$^+$ T cells. Cells were analyzed on a

Cytek Aurora spectral flow cytometer. The percent and number of S-specific $CD45^+CD4^+CD44^+CD62L^-CD69^+$ T cells (A and B), IFNγ+ (C and D), IL-17+ (E and F), and IL-5+ (G and H) producing $CD4^+$ T cells are shown in A-H. The percent and number of PMA/Ionomycin-stimulated $CD45^+CD4^+CD44^+CD62L^-CD69^+$ T cells (I and J), $IFN\gamma^+$ (K and L), $IL\text{-}17^+$ (M and N), and $IL\text{-}5^+$ (O and P) producing $CD4^+$ T cells are shown in I-P. One-way ANOVA with Tukey's multiple comparisons was used to detect differences among groups ($*P < 0.05$; $**P < 0.01$; $***P < 0.001$; $****P < 0.0001$).

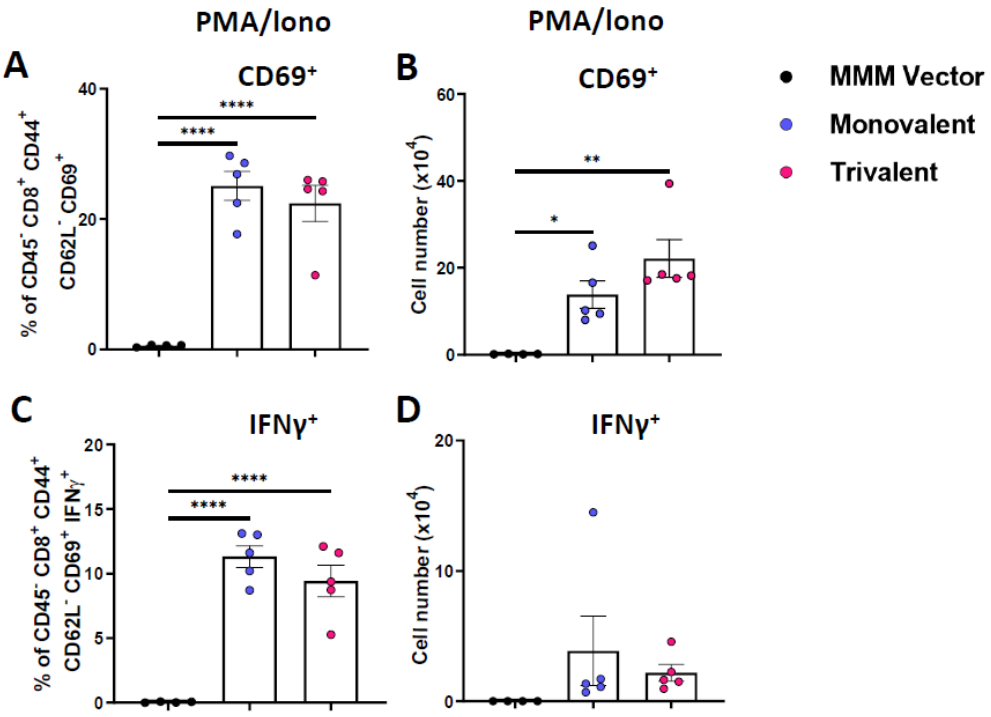

Fig.S6. Monovalent and trivalent vaccines induce CD8$^+$ T cell immune responses in the lungs after stimulation with PMA/Ionomycin. The CD8$^+$CD69$^+$ T cells in the lungs form **Fig.5** were stimulated PMA/Ionomycin in the presence of protein transport inhibitors. The percent and number of PMA/Ionomycin-stimulated-specific CD45$^-$CD8$^+$CD44$^+$CD62L$^-$ CD69$^+$ T cells (A and B), IFNγ$^+$-producing CD8+ T cells (C and D) are shown. One-way ANOVA with Tukey's multiple comparisons was used to detect differences among groups (*$P < 0.05$; ****$P < 0.0001$).

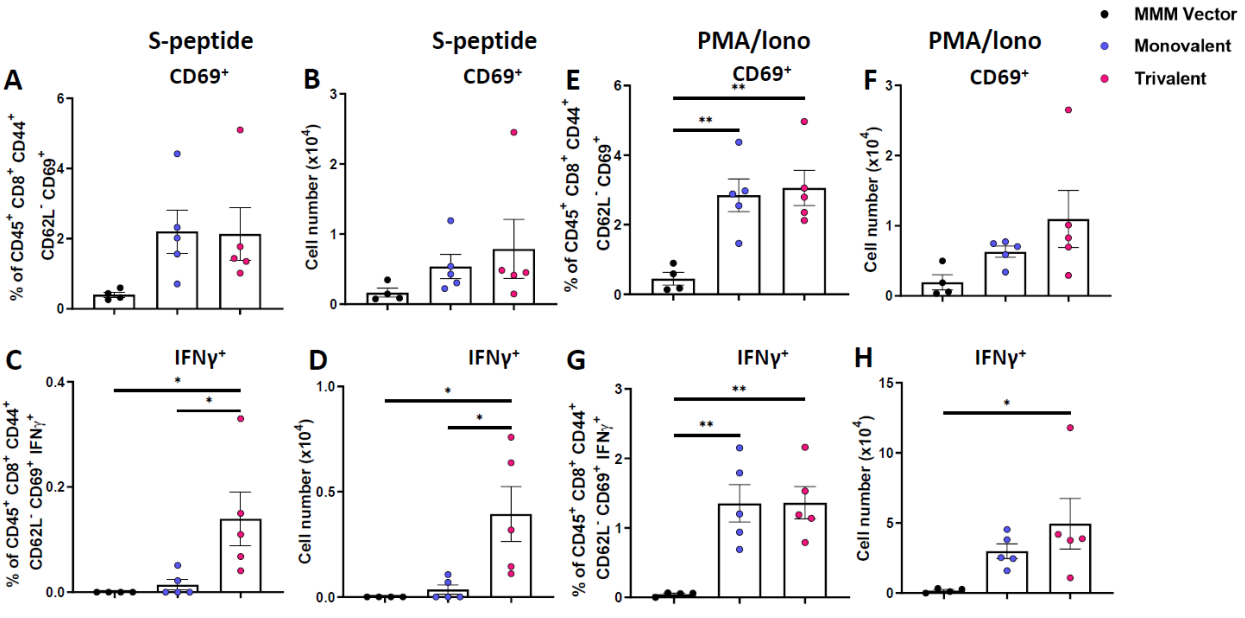

Fig.S7. Monovalent and trivalent vaccines induce circulating CD8$^+$ T cell immune responses in the lungs. The CD8$^+$CD69$^+$ T cells in the lungs were stimulated WA1 S peptide or PMA/Ionomycin. The percent and number of S-specific CD45$^+$CD8$^+$CD44$^+$CD62L$^-$CD69$^+$ T cells (A and B), IFNγ$^+$-producing CD8$^+$ T cells (C and D), and the percent and number of PMA/Ionomycin-stimulated-specific CD45$^+$CD8$^+$CD44$^+$CD62L$^-$ CD69$^+$ T cells (E and F), IFNγ$^+$-producing CD8$^+$ T cells (G and H) are shown. One-way ANOVA with Tukey's multiple comparisons was used to detect differences among groups (*$P < 0.05$; ****$P < 0.0001$).

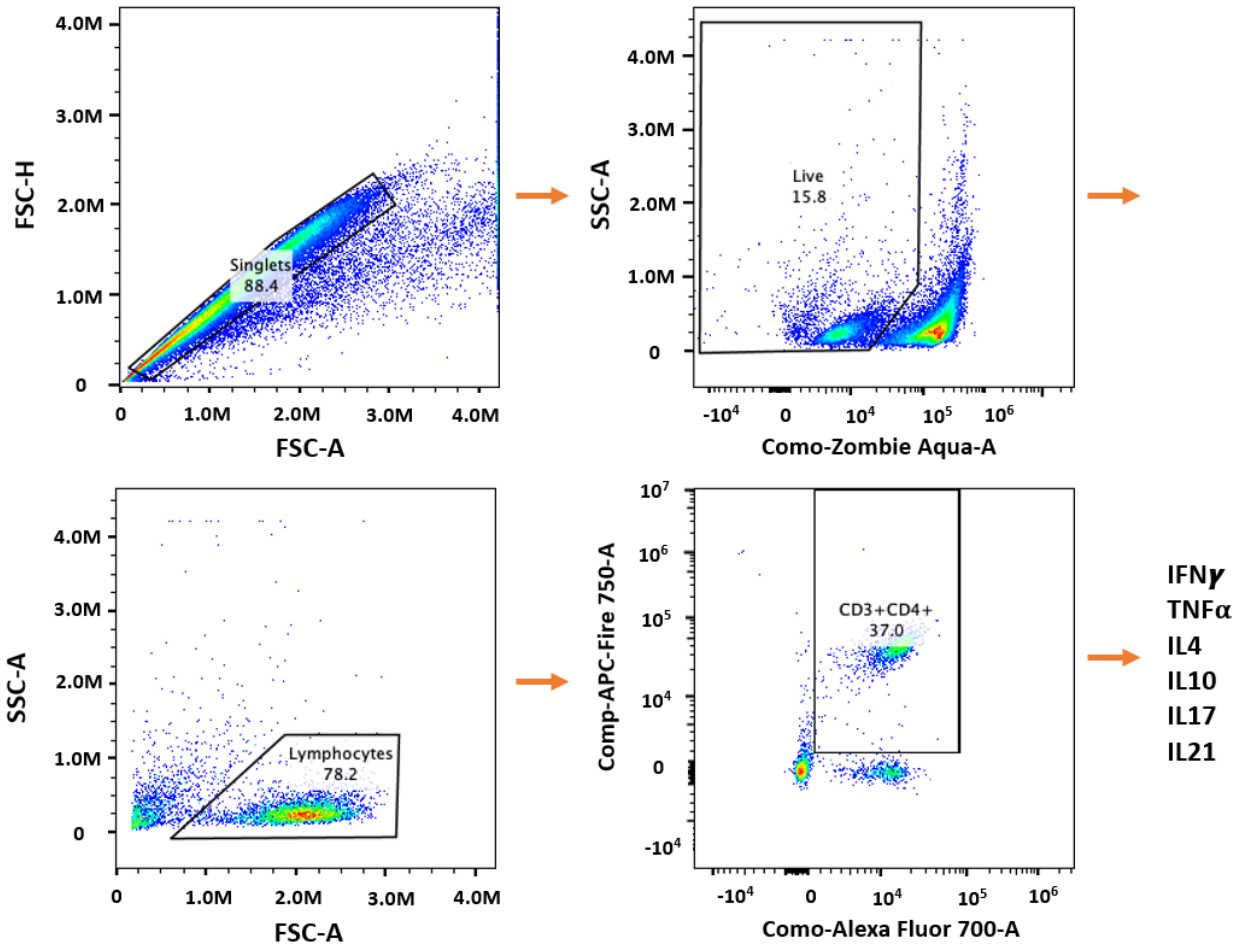

Fig.S8. Gating strategy for characterization of antigen-specific T cells producing cytokines in spleen cells after stimulation with S-specific peptide in intracellular cytokine staining (ICS) assay.

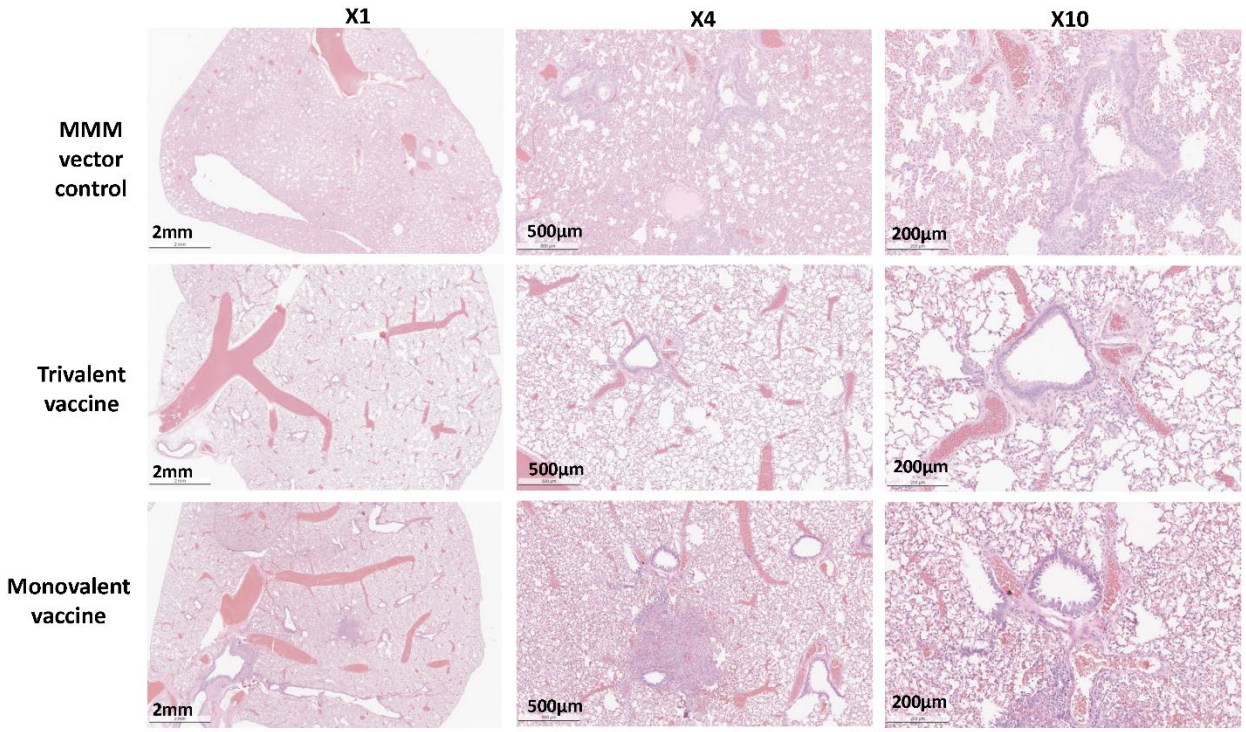

Fig.S9. Monovalent and trivalent immunization protects against lung pathology. Hamsters were euthanized at day 4 after SARS-CoV-2 WA1 challenge. Lung tissue was stained with hematoxylin/eosin. Micrographs with 1×, 4×, and 10× magnification of a representative lung section from each group are shown. Scale bars are indicated at the left corner of each image.

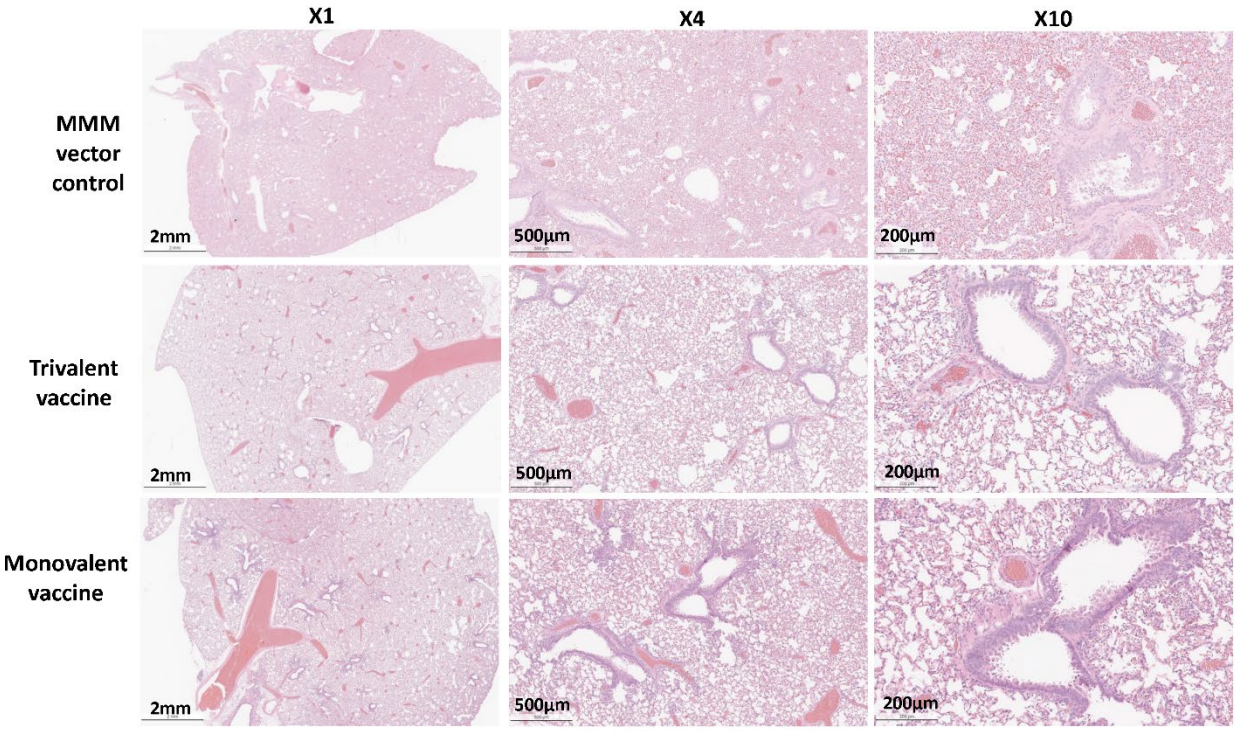

Fig.S10. Monovalent and trivalent immunization protects against lung pathology. Hamsters were euthanized at day 4 after SARS-CoV-2 Delta variant challenge. Lung tissue was stained with Hematoxylin/eosin. Micrographs with 1×, 4×, and 10× magnification of a representative lung section from each group are shown. Scale bars are indicated at the left corner of each image.

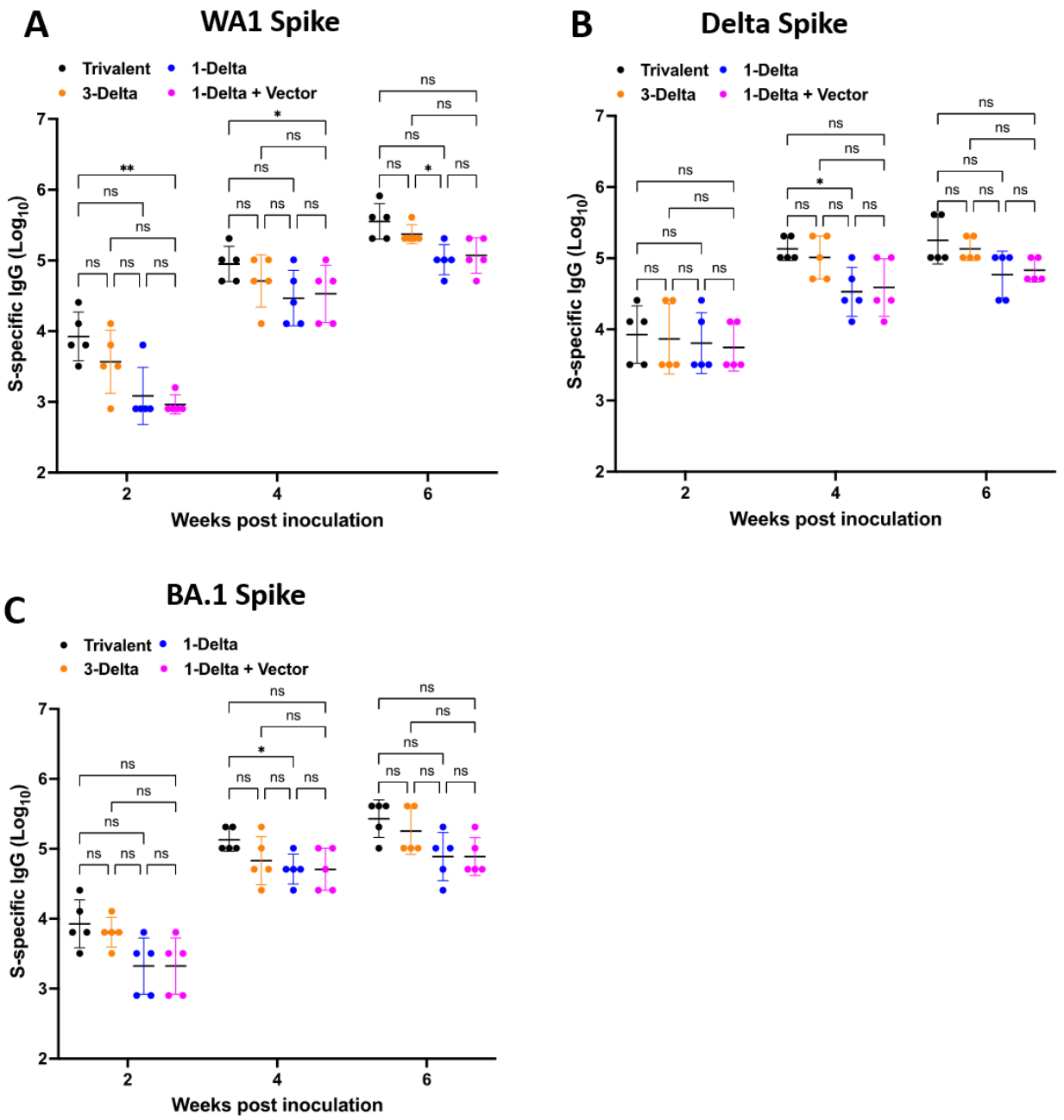

- Trivalent: a mixture of 5x10^5 PFU of rMuV-JL1-Delta-preS-6P, 5x10^5 PFU of rMuV-JL2-WA1-preS-6P, and 5x10^5 PFU of rMeV-BA.1-preS-6P
- 3-Delta: 1.5×10^6 PFU of rMuV-JL1-Delta-preS-6P
- 1-Delta: 5x10^5 PFU of rMuV-JL1-Delta-preS-6P
- 1-Delta+Vector: a mixture of 5x10^5 PFU of rMuV-JL1-Delta-preS-6P, 5x10^5 PFU of rMuV-JL2, and 5x10^5 PFU of rMeV

Fig.S11. rMeV and rMuV vectors do not interfere with the S-specific antibody induced by

rMuV-JL1-Delta-preS-6P. IFNAR1$^{-/-}$mice were intranasally immunized with 1.5×10^6 PFU of trivalent vaccine (5×10^5 PFU of rMuV-JL1-Delta-preS-6P, rMuV-JL2-WA1-preS-6P, and rMeV-BA.1-preS-6P), 1.5×10^6 PFU of rMuV-JL1-Delta-preS-6P, 5×10^5 PFU of rMuV-JL1-Delta-preS-6P, or 1.5×10^6 PFU of rMuV-JL1-Delta-preS-6P+Vector (5×10^5 PFU of rMuV-JL1-Delta-preS-6P, rMuV-JL2, and rMeV). At week 3, each group was boosted with the same vaccine at the same dose. At weeks 2, 4, and 6, serum was collected from each mouse for detection of IgG antibody by ELISA using preS-6P of SARS-CoV-2 WA1 (A), Delta variant (B), or Omicron BA.1 (C) as the coating antigen. Data shown are the GMT of five mice ± SD. Data were analyzed using two-way ANOVA (*$P < 0.05$; **$P < 0.01$; ***$P < 0.001$; ****$P < 0.0001$).

Additional Discussion

MMR vaccine is one of the most successful vaccines in human history, inducing life-long protection. This combination virus vaccine has been used in infants and children since 1971, but the component vaccines were approved in 1963 (MeV), 1967 (MuV), and 1969 (rubella). Both MeV and MuV are excellent vaccine vectors. Using reverse genetics, a foreign gene can be inserted into the genome of MeV or MuV as an additional transcription unit. Recombinant virus expressing that foreign protein can induce strong systemic immune responses. The MMR vaccine contains four attenuated virus strains, MeV, MuV-JL1, MuV-JL2, and rubella virus. Therefore, three viruses (MeV, MuV-JL1, and MuV-JL2) in the MMR vaccine could be modified to express a different antigen as components of a trivalent vaccine candidate. Our MMS vaccine is a multivalent COVID-19 vaccine containing three optimized preS-6P proteins (one preS-6P from the original SARS-CoV-2 strain and two preS-6P from recently identified Delta and Omicron BA.1 VoCs) which are incorporated into MuV-JL2, MuV-JL1, and MeV, respectively.

preS-6P-based antigen is more immunogenic than preS-2P-based antigen. We have demonstrated that preS-6P is significantly more immunogenic than preS-2P in three non-segmented negative sense (NNS) RNA viral vectors including MuV (11), MeV(3), vesicular stomatitis virus (VSV)(12). For example, sera raised by rMeV-preS-6P and rMuV-preS-6P had 6 and 8.5-fold more neutralizing antibody compared to rMeV-preS-2P and rMuV-preS-2P, respectively (3, 11). Antibodies induced by rVSV-preS-6P neutralized SARS-CoV-2 VoCs 2-4-fold more efficiently than those induced by rVSV-preS-2P (12). These studies highlight the importance of using preS-6P in the next generation COVID-19 vaccine.

In March of 2021, Merck discontinued the development of rMeV-based COVID-19 vaccine (V591 or TMV-083) which is a MeV Schwarz strain expressing the full-length S with 2 prolines (with deleted furin cleavage site and two mutations in the endoplasmic reticulum retrieval signal) inserted at the H-L gene junction in the genome (13, 14). It should be noted that our rMeV-preS-2P reported previously (4) and rMeV-preS-6P reported here are different from V591 (13, 14) and MV-ATU2-SF-2P-dER (15). The preS-2P and preS-6P that we used have a deletion in the furin cleavage site that prevents cleavage and its TM/CT domains are replaced by a foldon domain to further stabilize the protein and enable it to be secreted (1, 16). Given the fact that the preS-6P-based vaccine constructs are much more immunogenic than the preS-2P-based vaccine candidate, the immunogenicity protective capabilities of rMeV-preS-6P should be tested clinically.

Intranasal delivery of MMS vaccine and mucosal immunity. We found that intranasal delivery of MMS vaccine is superior to subcutaneous immunization at inducing higher serum IgG and SARS-CoV-2-specific IgA enriched at mucosal surfaces that are sampled in BAL. In contrast, subcutaneous immunization does not induce any detectable IgA in the blood or lungs. In addition, we showed that intranasal immunization of MMS vaccine alone induced a strong systemic and mucosal immune response and provided complete protection against challenge with the ancestral SARS-CoV-2 WA1, Delta variant, and Omicron BA.1 variant. Secretory IgA (sIgA) at the mucosal surface plays a critical role in immune defense by enabling neutrophils to undergo NETosis which traps and kills virus, thereby limiting spread (17, 18). In addition, sIgA provides superior protection against both homologous and heterologous virus infection than circulating IgG antibodies alone (17, 18). Thus, such a next-generation COVID-19 should induce strong serum and mucosal

589 antibodies which are essential for preventing SARS-CoV-2 infection and transmission.

590

591 Another advantage of using an intranasal vaccine is the ability to induce T_{RM}, that significantly
592 accelerate the recognition and clearance of pathogens previously encountered at that site. We
593 showed that intranasal delivery of monovalent and trivalent vaccines induce lung T_{RM} cells, the
594 hallmark of an effective mucosal respiratory vaccine. Both the monovalent and trivalent vaccines
595 induced $CD4^+$Th1 (IFN-γ), $CD4^+$Th17 (IL17), and $CD8^+$ T (IFN-γ) cells, but rarely $CD4^+$Th2 (IL-
596 5) cells. Our previous animal immunization experiments using rMuV-preS-6P demonstrated that
597 intranasal but not subcutaneous immunization induces SARS-CoV-2-specific lung T_{RM} cells (11).
598 The superior ability of T_{RM} cells to provide antiviral protection probably results from their ability
599 to immediately respond to invading pathogens owing to their location, either through cell-intrinsic
600 protective mechanisms (cytolysis, cytokine secretion) or by recruiting circulating cell subsets
601 (chemokine induction) (19). In a naturally infected individual, SARS-CoV-2–specific memory T
602 and B cells are localized preferentially to lung and lung-associated lymph nodes, providing direct
603 evidence that those sites are key locations for establishing immune memory after SARS-CoV-2
604 infection (20). The IFN-γ–producing $CD4^+$ and $CD8^+$ T_{RM} cells have been shown to broadly
605 enhance tissue-wide antiviral responses such as the upregulation of type I IFN signaling pathway
606 factors and enhanced leukocyte recruitment to the site of infection (21).

607

608 CDC and FDA recommend MMR vaccine be administered subcutaneously or intramuscularly.
609 However, several human trials demonstrated that intranasal delivery of MeV and MuV are safe
610 and highly efficacious. Human clinical trials involving 2,887 individuals showed that aerosolized
611 MeV vaccine (MeV Edmonston-Zagreb and Schwarz strains) was safe and more immunogenic

than subcutaneous vaccine (22, 23). In 1997, nearly 4 million schoolchildren in Mexico were immunized intranasally with MeV vaccine with high apparent effectiveness and safety (22). In non-human primates, intranasal immunization of MeV vaccine led to MeV replication in the muscle, nasal tissues, lungs, and draining lymph nodes which elicited optimal immunity and protection (24). Similarly, intranasal vaccination of the MuV L-3 vaccine strain induced higher MuV-neutralizing antibody titers in human volunteers than other immunization routes (25) .

Non-segmented negative-sense (NNS) RNA viruses as vectors to deliver SARS-CoV-2 vaccines. NNS RNA viruses have strong potential to be used as vectors for development of the next generation vaccine for SARS-CoV-2. Many NNS RNA viruses such as pneumoviruses (e.g. human respiratory syncytial virus, RSV), human paramyxoviruses [e.g. MeV, MuV, human parainfluenza virus 3 (PIV3)] or animal paramyxoviruses (parainfluenza virus 5, PIV5; Newcastle disease virus, NDV; avian paramyxovirus type 3, APMV3) are natural respiratory viruses which can be developed as intranasal vectored vaccines. Among them, a phase I clinical trial of an NDV-preS-6P-based COVID-19 vaccine candidate (NDV-HXP-S) has a high safety and immunogenicity profile (26, 27). In addition, RSV-S (replacement of RSV glycoproteins with native full-length S) (28) and PIV5-S (PIV5 expressing native full-length S)-based COVID-19 vaccine candidates (29) are currently being evaluated as intranasal vaccines in human clinical trials.

References

1. C. L. Hsieh *et al.*, Structure-based design of prefusion-stabilized SARS-CoV-2 spikes. *Science* **369**, 1501-+ (2020).
2. Y. Zhang *et al.*, A highly efficacious live attenuated mumps virus-based SARS-CoV-2 vaccine candidate expressing a six-proline stabilized prefusion spike. *P Natl Acad Sci USA* **119** (2022).
3. Y. Zhang *et al.*, Recombinant measles virus expressing prefusion spike protein stabilized by six rather than two prolines is more efficacious against SARS-CoV-2 infection. *J Med*

Virol 10.1002/jmv.28687 (2023).
4. M. J. Lu *et al.*, A safe and highly efficacious measles virus-based vaccine expressing SARS-CoV-2 stabilized prefusion spike. *P Natl Acad Sci USA* **118** (2021).
5. T. R. Fuerst, E. G. Niles, F. W. Studier, B. Moss, Eukaryotic Transient-Expression System Based on Recombinant Vaccinia Virus That Synthesizes Bacteriophage-T7 Rna-Polymerase. *P Natl Acad Sci USA* **83**, 8122-8126 (1986).
6. C. Zeng *et al.*, Neutralizing antibody against SARS-CoV-2 spike in COVID-19 patients, health care workers, and convalescent plasma donors. *Jci Insight* **5** (2020).
7. J. P. Evans *et al.*, Neutralization of SARS-CoV-2 Omicron sub-lineages BA.1, BA.1.1, and BA.2. *Cell Host Microbe* **30**, 1093-1102 e1093 (2022).
8. P. Qu *et al.*, Neutralization of the SARS-CoV-2 Omicron BA.4/5 and BA.2.12.1 Subvariants. *New Engl J Med* **386**, 2526-+ (2022).
9. W. Su *et al.*, Reduced Pathogenicity and Transmission Potential of Omicron BA.1 and BA.2 Sublineages Compared with the Early Severe Acute Respiratory Syndrome Coronavirus 2 D614G Variant in Syrian Hamsters. *J Infect Dis* **227**, 1143-1152 (2023).
10. K. G. Anderson *et al.*, Intravascular staining for discrimination of vascular and tissue leukocytes. *Nat Protoc* **9**, 209-222 (2014).
11. Y. Zhang *et al.*, A highly efficacious live attenuated mumps virus-based SARS-CoV-2 vaccine candidate expressing a six-proline stabilized prefusion spike. *Proc Natl Acad Sci U S A* **119**, e2201616119 (2022).
12. M. Lu *et al.*, SARS-CoV-2 prefusion spike protein stabilized by six rather than two prolines is more potent for inducing antibodies that neutralize viral variants of concern. *Proc Natl Acad Sci U S A* **119**, e2110105119 (2022).
13. O. Launay *et al.*, Safety and immunogenicity of a measles-vectored SARS-CoV-2 vaccine candidate, V591 / TMV-083, in healthy adults: results of a randomized, placebo-controlled Phase I study. *Ebiomedicine* **75** (2022).
14. F. Vanhoutte *et al.*, Safety and immunogenicity of the measles vector-based SARS-CoV-2 vaccine candidate, V591, in adults: results from a phase 1/2 randomised, double-blind, placebo-controlled, dose-ranging trial. *Ebiomedicine* **75** (2022).
15. P. N. Frantz *et al.*, A live measles-vectored COVID-19 vaccine induces strong immunity and protection from SARS-CoV-2 challenge in mice and hamsters. *Nat Commun* **12** (2021).
16. D. Wrapp *et al.*, Cryo-EM structure of the 2019-nCoV spike in the prefusion conformation. *Science* **367**, 1260-+ (2020).
17. H. D. Stacey *et al.*, IgA potentiates NETosis in response to viral infection. *P Natl Acad Sci USA* **118** (2021).
18. Y. H. Jang *et al.*, Cold-adapted pandemic 2009 H1N1 influenza virus live vaccine elicits cross-reactive immune responses against seasonal and H5 influenza A viruses. *J Virol* **86**, 5953-5958 (2012).
19. L. Chen, B. Wei, D. L. Di, A narrative review of tissue-resident memory T cells and their role in immune surveillance and COVID-19. *Eur Rev Med Pharmaco* **26**, 4486-4496 (2022).
20. M. M. L. Poon *et al.*, SARS-CoV-2 infection generates tissue-localized immunological memory in humans. *Sci Immunol* **6** (2021).
21. S. L. Urban *et al.*, Peripherally induced brain tissue-resident memory CD8(+)T cells mediate protection against CNS infection. *Nat Immunol* **21**, 938-+ (2020).
22. N. Low, S. Kraemer, M. Schneider, A. M. H. Restrepo, Immunogenicity and safety of

aerosolized measles vaccine: Systematic review and meta-analysis. *Vaccine* **26**, 383-398 (2008).
23. J. V. Bennett *et al.*, Aerosolized measles and measles-rubella vaccines induce better measles antibody booster responses than injected vaccines: randomized trials in Mexican schoolchildren. *B World Health Organ* **80**, 806-812 (2002).
24. R. L. de Swart *et al.*, Needle-free delivery of measles virus vaccine to the lower respiratory tract of non-human primates elicits optimal immunity and protection. *Npj Vaccines* **2** (2017).
25. V. P. Krasnova, N. V. Iuminova, V. A. Liashenko, [An intranasal method of revaccination against mumps]. *Vopr Virusol* **39**, 24-26 (1994).
26. P. Pitisuttithum *et al.*, Safety and immunogenicity of an inactivated recombinant Newcastle disease virus vaccine expressing SARS-CoV-2 spike: Interim results of a randomised, placebo-controlled, phase 1 trial. *Eclinicalmedicine* **45** (2022).
27. A. D. Dang *et al.*, Safety and immunogenicity of an egg-based inactivated Newcastle disease virus vaccine expressing SARS-CoV-2 spike: Interim results of a randomized, placebo-controlled, phase 1/2 trial in Vietnam. *Vaccine* **40**, 3621-3632 (2022).
28. M. F. Tioni *et al.*, Mucosal administration of a live attenuated recombinant COVID-19 vaccine protects nonhuman primates from SARS-CoV-2. *Npj Vaccines* **7** (2022).
29. D. An *et al.*, Protection of K18-hACE2 mice and ferrets against SARS-CoV-2 challenge by a single-dose mucosal immunization with a parainfluenza virus 5-based COVID-19 vaccine. *Sci Adv* **7** (2021).